Impact of Climate Change and High PV Penetration on Power Factor Profile

Arif Ahmed*, Tobias Massier†

*†TUMCREATE Ltd., Singapore 138602

Email: *arif.ahmed@tum-create.edu.sg, †tobias.massier@tum-create.edu.sg

Abstract—One of the highest uptake rates observed in recent years in distributed generation technologies to tackle climate change is the solar photovoltaic (PV) systems. However, the growing number of PV systems deployed in power networks can adversely impact the grid. The effect on the network power factor profile, which is a key indicator of voltage stability that is recommended to be maintained within a predefined margin, is one of the adverse impacts of high uptake of PV systems. This manuscript presents an impact study of climate change and high PV penetration on power factor profile using the recently proposed weather-dependent power flow (WDPF) algorithm. The WDPF algorithm accurately takes into account the effect of weather into power flow analysis using the nonlinear heat balance model of overhead conductors. The WDPF algorithm, in this manuscript, is utilised to investigate the power factor profile paired with the impact of climate change and high PV penetration on the IEEE 14-bus network. Simulation performed on the IEEE 14-bus network shows convincing results and the benefit of using the WDPF algorithm.

Index Terms—Distributed PV, Photovoltaic systems, Weather-dependent power flow, PV Integration, Power factor profiling

I. Introduction

The rapidly growing energy demand requires fast extension of the power generation system. Fossil fuels such as coal and gas are still the main sources of electricity generation, with a share of more than 60% [1]. Consequently, greenhouse gas emissions have been increasing, reaching $32.5\,\text{Gt}$ of CO_2 alone in 2017 [1]. Particularly the past 40 years saw a high increase of the atmospheric concentration of greenhouse gases and consequently temperatures [2].

To mitigate these changes, more and more alternative emission-free or emission-neutral forms of electricity generation are being deployed. Hydro power, wind power or solar photovoltaics (PV) are some examples.

PV systems have grown at an average annual rate of around 60% in recent years and has quickly become an important part of modern power systems [3]. The increasing penetration of PV systems into the power grid presents numerous challenges including voltage rise, reverse power flow, voltage instability, network power loss, etc. [4]–[6]. As the penetration of PV systems into the grid continues to rise, the importance of accurate modeling and analysis is becoming increasingly relevant to understand the impacts on the grid.

An important impact of high PV penetration on the grid is the variation in power factor profile of the network. This is mainly due to active power injection of PV systems into the grid that increases the real and reactive power imbalance leading to poor power factors during the injections [4], [7], [8]. Power factor is an important indicator of voltage stability of a network and should not violate the recommended range [9], [10]. Poor power factor can lead to voltage instability and even voltage collapse [4].

The impact of high PV penetration has been discussed in the literature. In [11], the authors investigated the impact of high PV penetration on a large interconnected system. Both improvements and adverse effects of high PV penetration were identified. The nature of the impact of high PV penetration is determined by a number of factors like the penetration level, system topology, type of the disturbance as well as the location of a fault. Greater voltage dips following disturbances were observed with high PV penetration levels. Another study [12] showed that high PV penetration leads to voltage deviation, voltage rise, and reverse power flows in the network. The impact of PV on power factor profiles is also found in the literature. In [13], the impact of centralized PV systems with various power factor control schemes on utility power factor profiles was investigated. The authors showed that optimally placed PV systems with power factor schedule can improve the power factor profile of the network and enhance the stability of the grid. The aforementioned studies show the importance of impact assessment of high PV penetration is on the power grid.

Most studies in the literature assess impacts of PV using the conventional power flow (PF) algorithm, which does not take into account the impact of varying weather conditions. In [14], the authors studied the impacts of PV in a power network utilising the temperature-dependent power flow (TDPF) that uses the ambient temperature data for a more accurate power flow analysis. The time-series power flow analysis undertaken in [14] showed significant differences in network losses, and changes in voltage magnitudes were also observed due to the consideration of the ambient temperature data. However, the TDPF algorithm utilises a linear thermal resistance model, which does not fully incorporate the nonlinear effects of weather on the conductor temperature described by the heat balance model [15].

To address this problem, the weather-dependent power flow (WDPF) algorithm was recently proposed and presented that is explicitly parameterised in terms of commonly available and measured weather parameters [16]. The WDPF algorithm fully incorporates the nonlinear effects of weather on the conductor

temperature and therefore performs a more accurate power flow analysis.

In this manuscript, we address the gap of an accurate analysis of high PV penetration by focusing on the collective impacts of weather and high PV penetration on the network power factor profile. Furthermore, we also investigate the impact of climate change and high PV penetration on the power factor profile using the WDPF algorithm. Simulation study on the IEEE 14-bus network is carried out to investigate these impacts considering a month-long weather dataset of New Zealand and utilizing the WDPF algorithm.

Section II of the manuscript presents the overview of the WDPF algorithm, Section III discusses the solar PV modeling and solar data used in the study followed by Section IV, which presents the IEEE 14-Bus network for simulation study. Simulation details are presented in Section V, simulation results are presented and discussed in Section VI and the manuscript is concluded in Section VII.

II. OVERVIEW OF WEATHER-DEPENDENT POWER FLOW

The WDPF algorithm utilises the steady-state nonlinear heat balance model of overhead conductors presented in the IEEE Std 738$^{\text{TM}}$-2012 [15] to fully incorporate the effects of weather into power flow analysis. The steady-state nonlinear heat balance model is as presented in Equation (1). Details of the expressions of Equation (1) should be referred to in [15], [16].

$$q_c + q_r = q_s + q_j \tag{1}$$

In Equation (1), q_c is the convective cooling rate in (W/m), q_r is the radiative cooling rate in (W/m), q_s is the solar heat gain rate in (W/m), and q_j is the Joule heat gain rate in (W/m).

The Joule heat gain (q_j) in a conductor is equal to the resistive losses ($I^2 R$) of the conductor. Therefore, q_j in Equation (1), for any conductor between Bus i and Bus j can be written as:

$$q_{j_{ij}} = (E_i^2 + E_j^2 + F_i^2 + F_j^2 - 2E_iE_j - 2F_iF_j)g_{ij} \tag{2}$$

In Equation (2), E_i is the real part of the complex voltage at Bus i, E_j is the real part of the complex voltage at Bus j, F_i is the imaginary part of the complex voltage at Bus i, F_j is the imaginary part of the complex voltage at Bus j, and g_{ij} is the branch conductance.

The heat balance of a conductor between Bus i and Bus j is thus derived by the substitution of Equation (2) in Equation (1), which yields Equation (3).

The nonlinear heat balance Equation (3) can be solved to calculate the conductor temperature ($T_{c_{ij}}$) given the weather conditions, conductor characteristics, and line loading.

Under steady-state condition, the nonlinear heat balance Equation (3), can be represented as a function conductor temperature as shown in Equation (4).

Based on Equation (4), a mismatch equation of the steady-state nonlinear heat balance is formed to calculate the conductor temperature (T_c) as represented in Equation (5).

$$\Delta H_{ij} = -H_{ij}^{calc} \tag{5}$$

In Equation (5), H_{ij}^{calc} is the calculated value of the nonlinear heat balance function.

Equation (5) is essential to deriving the WDPF algorithm. The heat balance mismatch vector is formed for all the weather-dependent branches in a network and then appended to the conventional power flow algorithm (PF) [5], [17], [18] to derive the update equation of the WDPF algorithm as:

$$\begin{bmatrix} \boldsymbol{E} \\ \boldsymbol{F} \\ \boldsymbol{T_c} \end{bmatrix}^{(v+1)} = \begin{bmatrix} \boldsymbol{E} \\ \boldsymbol{F} \\ \boldsymbol{T_c} \end{bmatrix}^{(v)} + \boldsymbol{J}^{-1(v)} \begin{bmatrix} \boldsymbol{\Delta P} \\ \boldsymbol{\Delta Q} \\ \boldsymbol{\Delta V^2} \\ \boldsymbol{\Delta H} \end{bmatrix}^{(v)} \tag{6}$$

In Equation (6), v is the iteration number, $\boldsymbol{\delta}$ is the vector of voltage angles, $\boldsymbol{V}$ is the vector of voltage magnitudes, $\boldsymbol{T_c}$ is the vector of weather-dependent branch temperatures, $\boldsymbol{\Delta P}$ is the vector of real power mismatch, $\boldsymbol{\Delta Q}$ is the vector of reactive power mismatch, and $\boldsymbol{\Delta H}$ is the heat balance mismatch vector. $\boldsymbol{J}$ in Equation (6) is defined as:

$$\boldsymbol{J}_{\text{new}} = \begin{bmatrix} \frac{\partial \boldsymbol{P}}{\partial \boldsymbol{E}} & \frac{\partial \boldsymbol{P}}{\partial \boldsymbol{F}} & \frac{\partial \boldsymbol{P}}{\partial \boldsymbol{T_c}} \\ \frac{\partial \boldsymbol{Q}}{\partial \boldsymbol{E}} & \frac{\partial \boldsymbol{Q}}{\partial \boldsymbol{F}} & \frac{\partial \boldsymbol{Q}}{\partial \boldsymbol{T_c}} \\ \frac{\partial \boldsymbol{V^2}}{\partial \boldsymbol{E}} & \frac{\partial \boldsymbol{V^2}}{\partial \boldsymbol{F}} & \frac{\partial \boldsymbol{V^2}}{\partial \boldsymbol{T_c}} \\ \frac{\partial \boldsymbol{H}}{\partial \boldsymbol{E}} & \frac{\partial \boldsymbol{H}}{\partial \boldsymbol{F}} & \frac{\partial \boldsymbol{H}}{\partial \boldsymbol{T_c}} \end{bmatrix} \tag{7}$$

The partial elements in the Jacobian ($\boldsymbol{J}$) in Equation (7), which are not included in the conventional PF, are given in [16]. As the WDPF algorithm considers the nonlinear heat balance model of overhead conductors, it is capable of accurately performing power flow analysis considering the weather conditions explicitly.

It should be noted that after every iteration in the power flow, given the calculated branch temperatures, the branch resistances are updated using Equation (8), as recommended in [16].

$$R(T_c) = \left[\left(\frac{R(T_{\text{high}}) - R(T_{\text{low}})}{T_{\text{high}} - T_{\text{low}}} \right) (T_c - T_{\text{low}}) + R(T_{\text{low}}) \right] \tag{8}$$

In Equation (8), $R(T_c)$ is the AC resistance at conductor temperature T_c, $R(T_{\text{high}})$ is the AC resistance at conductor temperature T_{high}, and $R(T_{\text{low}})$ is the AC resistance at conductor temperature T_{low}.

$$q_{c_{ij}} + q_{r_{ij}} = q_{s_{ij}} + (E_i^2 + E_j^2 + F_i^2 + F_j^2 - 2E_iE_j - 2F_iF_j)g_{ij} \tag{3}$$

$$H_{ij}(T_{c_{ij}}) = q_{c_{ij}} + q_{r_{ij}} - q_{s_{ij}} - (E_i^2 + E_j^2 + F_i^2 + F_j^2 - 2E_iE_j - 2F_iF_j)g_{ij} = 0 \tag{4}$$

III. Solar PV Modeling

A PV system connected to the grid is as shown in Fig. 1. The voltage at the output node of the PV is $\tilde{V}_{pv}$, the output
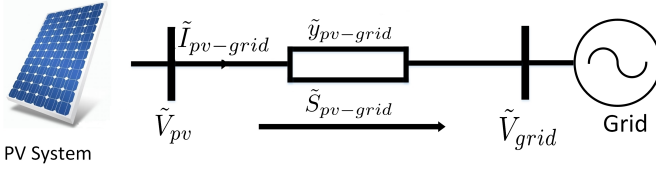

Fig. 1: Schematic representation of PV connected to the grid.

current at the node is $\tilde{I}_{pv-grid}$, which is given by:

$$\tilde{I}_{pv-grid} = (\tilde{V}_{pv} - \tilde{V}_{grid})\tilde{y}_{pv-grid} \quad (9)$$

The power injected into the grid is given by:

$$\tilde{S}_{pv-grid} = \tilde{V}_{pv}\tilde{I}^*_{pv-grid} \quad (10)$$

The power output of a PV system at unity power factor is given by [19]:

$$P_{pv} = P_{DC}\eta_{a} \quad (11)$$

where P_{DC} is the DC power generated by the PV cells due to the solar power input P_{input} such that $P_{DC} = P_{input}\eta_{mp}$, and η_{mp} is the maximum power-point efficiency. The generated DC power of a PV system depends on various parameters such as: ambient temperature, wind speed, PV cell temperature, Plane of Array (POA) irradiance, etc. [19]. η_{a} in Equation (11) is the efficiency of additional components of the PV system.

The maximum power-point efficiency (η_{mp}), which is temperature dependent [20] is given by:

$$\eta_{mp} = \eta_{ref}\left\{1 - \beta_{ref}\left[T_{a} - T_{ref} + (T_{NOCT} - T_{a,NOCT})\frac{G_{T}}{G_{NOCT}}\right]\right\} \quad (12)$$

In Equation (12), η_{ref} is the conversion efficiency at the standard test conditions, T_{a} is the ambient temperature, T_{ref} is the cell temperature at the standard test condition, T_{NOCT} is the nominal operating cell temperature, $T_{a,NOCT}$ is the ambient temperature under the nominal terrestrial environment, G_{T} is the incident radiation on the solar panel, and G_{NOCT} is the global solar flux under nominal terrestrial environment [19]. The PV system parameters used in the study are presented in Table I.

TABLE I: PV system parameters [6]

Parameter	Value
β_{ref}	0.004 $^\circ$C^{-1}
T_{ref}	25 $^\circ$C
T_{NOCT}	46 $^\circ$C
$T_{a,NOCT}$	20 $^\circ$C
G_{NOCT}	800 W/m^2
η_{ref}	0.8

In this manuscript, PV systems are considered to be injecting power at unity power factor and are modeled as PQ type [17] nodes for the power flow.

A. Solar Data

For the purpose of the study, real solar irradiance data from a weather station in the north island of New Zealand was collected from New Zealand's National Institute of Water and Atmospheric Research's (NIWA) for the month of January, 2016. The data collected was of 10 minute resolution and is presented in Fig. 2.
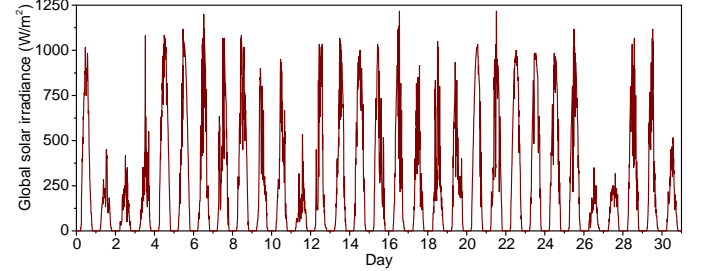

Fig. 2: Solar irradiance in January 2016.

IV. IEEE 14-Bus Test Network

For simulation, a modified IEEE 14-bus [21] system is considered as shown in Fig. 3. The modification here refers to the addition of PV systems at the load buses and increase in the loads and generations. All conductors in the modified IEEE 14-bus were considered to be the 795 kcmil 26/7 Drake ACSR conductor reported in IEEE Std 738^{TM}-2012 [15]. The original network data can be referred to in [21].
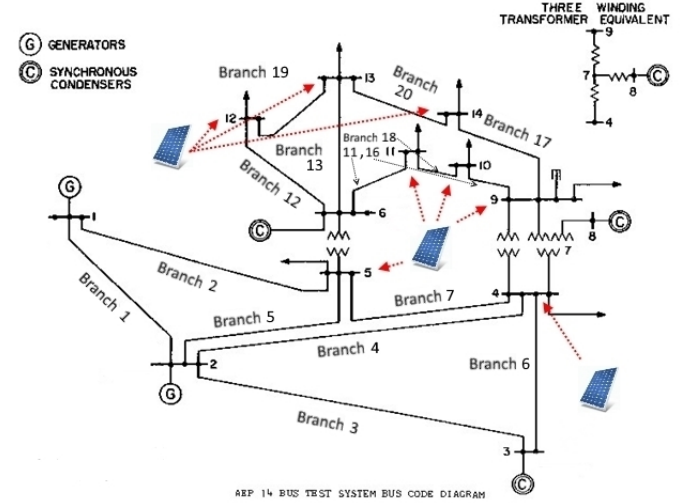

Fig. 3: Modified IEEE 14-Bus test network [21].

V. Simulation Details

For the purpose of simulation, a standard desktop computer was used and the algorithm was coded in MATLAB. To investigate the impact of climate change and high PV penetration, PV systems were deployed at 30% and 60% penetration level

at all the PQ nodes, respectively. The PV penetration level (p_k) at any Bus k here is defined as [22]:

$$p_k = \frac{\sum_{i=0}^{n} P_{pv_i}}{P_k} \tag{13}$$

where, P_{pv_i} is the AC rating of the ith PV system connected to the Bus k, n is the total number of PV systems connected to Bus k, and P_k is the peak load at Bus k.

The WDPF algorithm is utilised for the study, therefore the weather dataset for the month of January, 2016 was considered, which comprises of ambient temperature, wind speed, and incident wind angle in addition to the solar irradiance data as mentioned above.

To simulate the effect of climate change, two ambient temperature rise scenarios corresponding to a 5°C and a 10°C increase were considered. Therefore, the weather dataset considering a rise of 5°C and 10°C throughout the month was simulated with other weather parameters exhibiting no change.

A normalized load profile with a peak of 1 p.u. was obtained from [23] for the load buses in the network as presented in Fig. 5.
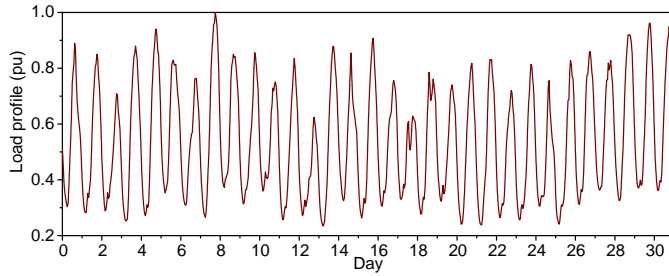

Fig. 4: Load profile for the PQ buses in network throughout the month.

All the branch temperatures were initialised with the ambient temperature, and simulations were carried out for every weather data point using the WDPF algorithm.

VI. SIMULATION RESULTS

A. Impact of high PV penetration in presence of weather

Integration of PV into the grid affects the power transfers of various branches in a network. Fig. 5 shows the power transfer for the month due to the various PV penetration levels in Branch 4, which connects the two highest loaded buses i.e. Bus 2 and Bus 4. As the PV penetration level increases, the power transfer in the branch reduces and the lowest troughs are observed for the highest PV penetration level of 60%. This is due to increased PV generation in Bus 4, which reduces the power requirement from the generator at Bus 2 and the Slack Bus. The lowest power transfer observed for 0% PV penetration, 30% PV penetration, and 60% PV penetration was 34.18 MW, 26.96 MW, and 6.85 MW, respectively.

The temperature of Branch 4 corresponding to Fig. 5 is presented in Fig. 6. It should be noted that the use of conventional power flow cannot yield branch temperatures
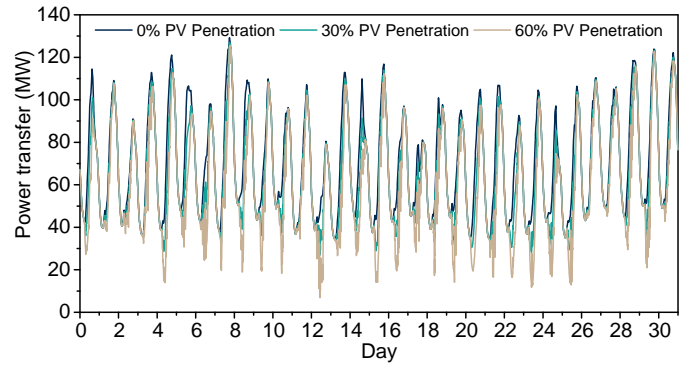

Fig. 5: Power transfer of Branch 4 for various PV penetration levels throughout the month.

based on power flow execution. In Fig. 6, the highest conductor temperature is seen for 0% PV penetration, while the lowest is observed for the 60% PV penetration. This is because at 60% PV penetration, less power is transferred from Bus 2, which results in lesser increase in the branch conductor temperature as compared to the 0% PV penetration scenario. The highest branch conductor temperature was 47.33°C for the 0% PV penetration scenario. The branch conductor temperature observed does not violate the thermal limit (100°C) of the conductor and therefore, the conductor operates in its safe thermal limit for all scenarios.
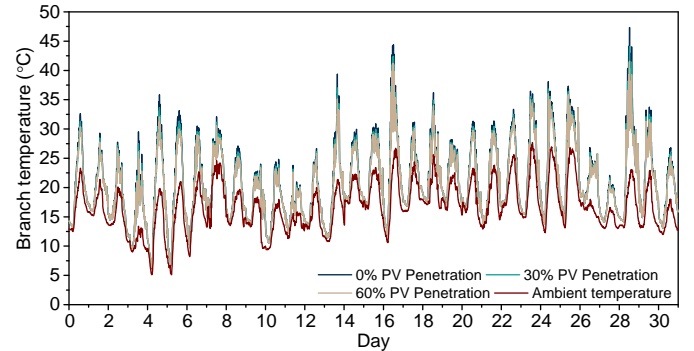

Fig. 6: Branch conductor temperature of Branch 4 for various PV penetration levels throughout the month.

The impact of increasing PV penetration on the power factor profile for the month is presented in Fig. 7. The power factor for the 0% and 30% PV penetration is within the acceptable range as observed in Fig. 7. However, the power factor reduces drastically to 0.65 on day 12 for the 60% PV penetration scenario. This is of concern to utilities as the generator at Bus 2 is required to supply more reactive power than active power.

B. Impact of climate change and high PV penetration

As stated before, two climate change scenarios are investigated i.e. a 5°C and a 10°C rise in the ambient temperature data. The power factor profile of Branch 4 due to the ambient temperature rise of 5°C and 10°C for 0% PV penetration level
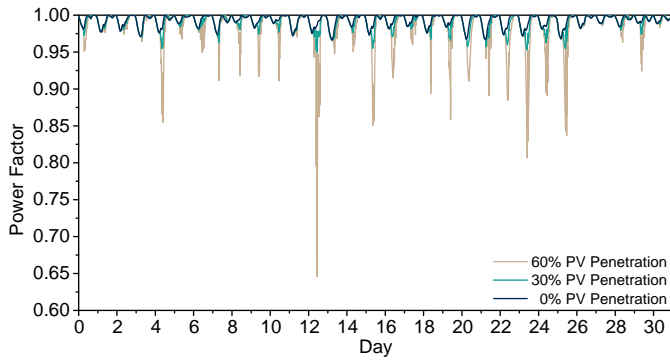
Fig. 7: Power factor profile of Branch 4 for various PV penetration levels throughout the month.

is presented in Figure 8. Similarly, the power factor profile for 30% PV penetration is presented in Figure 9.
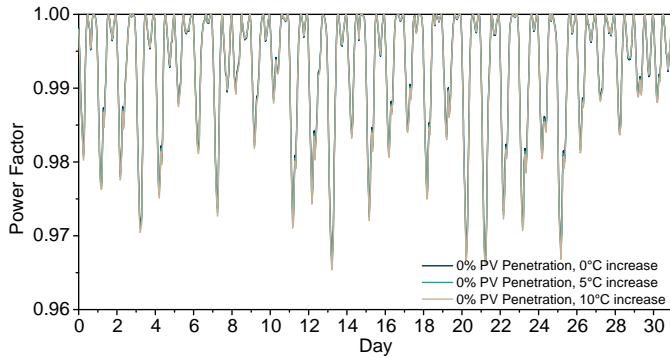

Fig. 8: Power factor profile of Branch 4 for 0% PV penetration with 0°C, 5°C, and 10°C rise in ambient temperature, respectively.
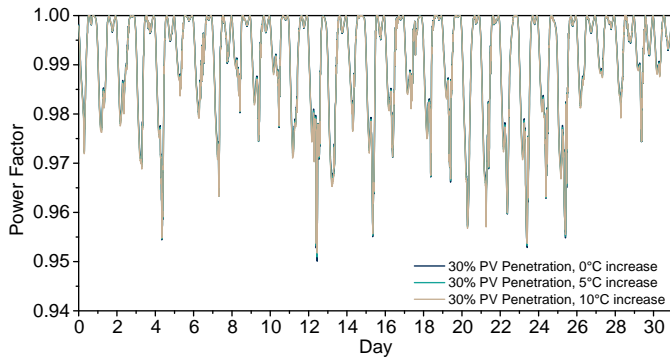

Fig. 9: Power factor profile of Branch 4 for 30% PV penetration with 0°C, 5°C, and 10°C rise in ambient temperature, respectively.

Negligible change in the power factor profile is observed in both 0% and 30% PV penetration scenarios due to increase in the ambient temperatures as seen in Fig. 8 and Fig. 9. The lowest power factor in Fig 8 and Fig. 9 for all the scenarios was around 0.96 and 0.95, respectively.

Fig. 10 presents the power factor profile of Branch 4 for 60% PV penetration in presence of rising ambient temperature. Higher impact on power factor profile is observed due to higher PV penetration in presence of rising ambient temperatures. The worst power factor on day 12 is observed for a 60% PV penetration with 0°C increase in ambient temperature, while the best power factor on day 12 is observed for a 60% PV penetration with 10°C increase in ambient temperature.
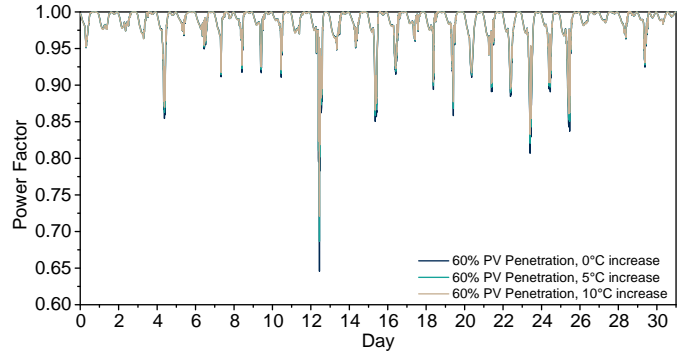

Fig. 10: Power factor profile of Branch 4 for 60% PV penetration with 0°C, 5°C, and 10°C rise in ambient temperature, respectively.

For a more clear understanding of the impact of 60% PV penetration with 10°C increase on day 12, the power transfer profile and the PV generation for the scenarios are presented in Fig. 11 and Fig. 12, respectively. In Fig. 11, as the ambient temperature increases, the peaks and troughs of the power transfer curves increases. This results in more real power transfer through the line and hence improving the power factor. Furthermore, as the ambient temperature rises in presence of high PV penetration (60%) in Fig. 12, the solar power generation peaks at Bus 4 are seen to reduce. This is due to the reduction in efficiency of solar generation as the ambient temperature raised by 10°C, which aided in improving the power factor profile of the branch. The lowest power factor observed for the 60% PV penetration with 10°C increase scenario was 0.72.
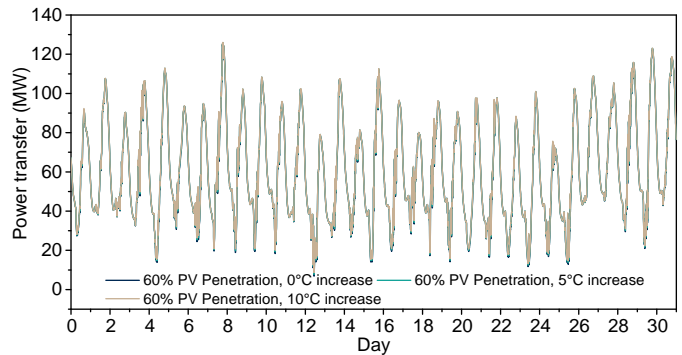

Fig. 11: Modified IEEE 14-Bus test network [21].

In summary, through the simulation case study and results, the impact of climate change and high PV penetration on the
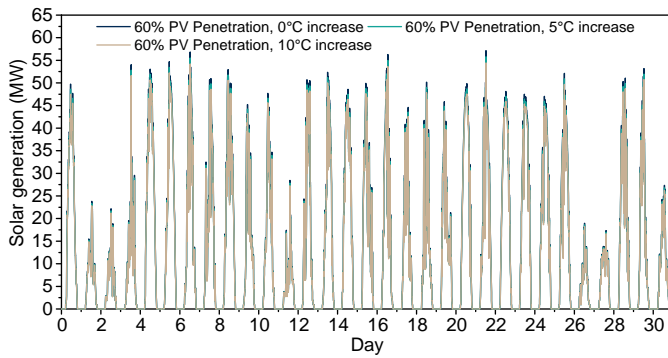
Fig. 12: Modified IEEE 14-Bus test network [21].

power factor profile has been assessed. The use of WDPF algorithm gives a more accurate and improved understanding of the impacts on the grid.

VII. CONCLUSION

The impact of high PV penetration in the presence of weather conditions has been assessed in this paper. It has been observed that high PV penetration reduces the source side branch power transfers. This causes a reduction of the branch temperature. On the other hand, high PV penetration adversely impacts the power factor profile of a branch.

Rising ambient temperature (a consequence of climate change) impacts on the power factor profile. It was observed that for similar load profiles, increased temperature and low PV penetration do not change the power factor profile noticeably. However, as the ambient temperature increases along with high PV penetration, noticeable changes are observed in the power factor profile. Lower variability in the power factor profile is observed in the high PV penetration scenario as the ambient temperature increases. Hence, an improvement is seen in comparison to 0°C rise in the ambient temperature scenario, which is due to the reduced solar generation efficiency at increased temperatures.

REFERENCES

[1] International Energy Agency, "Global energy & CO$_2$ status report," 2018, accessed 2019-03-15. [Online]. Available: https://goo.gl/4Lp3LJ

[2] The Intergovernmental Panel on Climate Change, "Climate change 2014: Synthesis report. contribution of working groups i, ii and iii to the fifth assessment report of the intergovernmental panel on climate change," The Intergovernmental Panel on Climate Change, Tech. Rep., 2014, accessed 2019-03-15. [Online]. Available: https://goo.gl/JZp6Xk

[3] S. Kouro, J. I. Leon, D. Vinnikov, and L. G. Franquelo, "Grid-connected photovoltaic systems: An overview of recent research and emerging pv converter technology," *IEEE Industrial Electronics Magazine*, vol. 9, no. 1, pp. 47–61, March 2015.

[4] M. H. Bollen and F. Hassan, *Integration of distributed generation in the power system*. John wiley & sons, 2011, vol. 80.

[5] O. Elgerd, *Electric Energy Systems Theory: An Introduction*. Tata McGraw-Hill, 1983.

[6] J. Widn, E. Wckelgrd, J. Paatero, and P. Lund, "Impacts of distributed photovoltaics on network voltages: Stochastic simulations of three swedish low-voltage distribution grids," *Electric Power Systems Research*, vol. 80, no. 12, pp. 1562 – 1571, 2010.

[7] P. González, E. Romero-Cadaval, E. González, and M. A. Guerrero, "Impact of grid connected photovoltaic system in the power quality of a distribution network," in *Doctoral Conference on Computing, Electrical and Industrial Systems*. Springer, 2011, pp. 466–473.

[8] M. ElNozahy and M. Salama, "Technical impacts of grid-connected photovoltaic systems on electrical networksa review," *Journal of Renewable and Sustainable Energy*, vol. 5, no. 3, p. 032702, 2013.

[9] P. Kundur, N. J. Balu, and M. G. Lauby, *Power system stability and control*. McGraw-hill New York, 1994, vol. 7.

[10] L. Lin, J. Wang, and W. Gao, "Effect of load power factor on voltage stability of distribution substation," in *2012 IEEE Power and Energy Society General Meeting*. IEEE, 2012, pp. 1–4.

[11] S. Eftekharnejad, V. Vittal, G. T. Heydt, B. Keel, and J. Loehr, "Impact of increased penetration of photovoltaic generation on power systems," *IEEE transactions on power systems*, vol. 28, no. 2, pp. 893–901, 2013.

[12] D. Cheng, B. Mather, R. Seguin, J. Hambrick, and R. P. Broadwater, "Pv impact assessment for very high penetration levels," in *2015 IEEE 42nd Photovoltaic Specialist Conference (PVSC)*. IEEE, 2015, pp. 1–6.

[13] M. Emmanuel, R. Rayudu, and I. Welch, "Impact of centralized photovoltaic systems on utility power factor profile using the wavelet variability model," in *2017 IEEE Innovative Smart Grid Technologies - Asia*, Dec 2017, pp. 1–6.

[14] A. Ahmed, F. S. McFadden, and R. Rayudu, "Impacts of distributed pv in a smart grid using temperature-dependent power flow," in *2017 IEEE Innovative Smart Grid Technologies-Asia*. IEEE, 2017, pp. 1–6.

[15] "IEEE standard for calculating the current-temperature relationship of bare overhead conductors," *IEEE Std 738-2012*, pp. 1–72, Dec 2013.

[16] A. Ahmed, F. J. S. McFadden, and R. K. Rayudu, "Weather-dependent power flow algorithm for accurate power system analysis under variable weather conditions," *IEEE Transactions on Power Systems*, 2019.

[17] H. Saadat, *Power System Analysis*. PSA Publishing, 2010.

[18] L. Powell, *Power System Load Flow Analysis*. McGraw-Hill Education, 2004.

[19] J. Duffie and W. Beckman, *Solar Engineering of Thermal Processes*, ser. A Wiley-Interscience Publication. Wiley, 1991.

[20] Q. Kou, S. Klein, and W. Beckman, "A method for estimating the long-term performance of direct-coupled pv pumping systems," *Solar Energy*, vol. 64, no. 1, pp. 33 – 40, 1998.

[21] "14 bus power flow test case, power systems test case archive," https://labs.ece.uw.edu/pstca/pf14/pg_tca14bus.htm.

[22] M. Ropp, J. Newmiller, C. Whitaker, and B. Norris, "Review of potential problems and utility concerns arising from high penetration levels of photovoltaics in distribution systems," in *2008 33rd IEEE Photovoltaic Specialists Conference*, May 2008, pp. 1–6.

[23] "OpenDSS - Electric Power Research Institute," https://www.epri.com/#/pages/sa/opendss?lang=en.